Vol. 36 (2005) ACTA PHYSICA POLONICA B No 11

PUZZLING b QUARK DECAYS: HOW TO ACCOUNT FOR THE CHARM MASS*

Andrzej Czarnecki, Alexey Pak, Maciej Ślusarczyk

Department of Physics, University of Alberta
Edmonton, AB T6G 2J1, Canada

(Received November 2, 2005)

For more than a decade, measurements of the semileptonic branching ratio of hadrons containing a b quark disagreed with the Standard Model predictions. Very recently, a class of strong-interaction effects was found to significantly increase the non-leptonic b decay rate and thus bring the Standard Model prediction into agreement with the experiment. Final state charm quark mass effects should be determined to refine the theoretical description of b decays. Prospects for such improvement are discussed in this talk.

PACS numbers: 13.25.Hw, 12.38.Bx, 14.65.Fy

1. Introduction

The b quark decays most frequently by giving rise to a charm quark and a virtual W boson. The W boson in turn can decay into one of the three possible leptonic channels, or into quarks. The former case is a semileptonic, the latter a hadronic (non-leptonic) decay of the b quark. It is easy to estimate the relative probability B_{SL} of a semileptonic decay with an electron in the final state, at least in the case when we neglect all interactions except the weak decay mechanism. First, neglect all masses of the final-state particles: we then have three semileptonic ($e\nu_e$, $\mu\nu_\mu$, $\tau\nu_\tau$) and two (ud or cs) times three (colors) hadronic channels. We find $B_{\mathrm{SL}}(b \to ce\nu_e) = 1/9 = 11\%$. In the opposite limit, if we consider c and τ as heavy and neglect their contribution to the virtual W decays, we get $B_{\mathrm{SL}}(b \to ce\nu_e) = 1/5 = 20\%$.

A more accurate account for the masses gives an intermediate value, $B_{\mathrm{SL}}(b \to ce\nu_e) \simeq (15-16)\%$ [1]. On the other hand, a measurement finds

* Presented at the XXIX International Conference of Theoretical Physics, "Matter to the Deepest", Ustroń, Poland, September 8–14, 2005.

for a B meson (one expects similar $B_{\rm SL}$ for the b quark as for a hadron containing it) [2]

$$B_{\rm SL}^{\rm exp}(B \to X e^+ \nu_e) = (10.91 \pm 0.26)\% \,. \tag{1}$$

The difference between the rather low experimental result and the theoretical prediction is mainly due to the strong interactions and until very recently was not well understood. Interestingly, most of those effects are perturbative [1] and thus a precise prediction can be made, provided multi-loop diagrams can be evaluated. Crucial effects are due to QED-like diagrams in which two gluons are exchanged between the quark line originating with the b quark and the line of quarks arising from the W decay. Those diagrams have been evaluated this year [3] in the limit in which the masses of the c quarks (as well as the lighter quarks) are neglected. In this limit theoretical prediction for the semileptonic branching ratio can be decreased to almost 11 percent, which is within one standard deviation from the experimantal value.

However, it has been pointed out that the charm quark mass can strongly alter the size of perturbative corrections, especially in the decay $b \to c\bar{c}s$ [4, 5]. The two charm quarks move slowly in much of the phase space of this decay and can be influenced by Coulomb-like interactions. It is very warranted to extend the analysis of [3] to evaluate the effect of the charm mass. This may be feasible if we apply the method of asymptotic operation [6]. In this talk its application is illustrated with the example of one-loop corrections to the muon decay, which is technically equivalent to the semileptonic b decay.

2. Example: muon decay and its radiative corrections

The electron mass effect in the muon decay is used here to illustrate the application of the ideas of asymptotic operation. Hopefully, this approach will lead in the future to the full knowledge of charm quark mass effects in b decays.

We adopt the following notation: M and m denote the muon and electron masses, $\rho = \frac{m}{M}$, and $\Gamma_0 = \frac{G_F^2 M^5}{192\pi^3}$. The W boson mass M_W is considered infinite (four-fermion theory). Calculations are performed in $D = 4-2\epsilon$ dimensions. We denote the common loop integration factor as $\mathcal{F}_0 = \frac{\Gamma(1+\epsilon)}{(4\pi)^{D/2} M^{2\epsilon}}$. In the expansions we keep terms up to ρ^6 and ϵ^0.

3. Tree level decay rate

The optical theorem is used to compute the decay width from the imaginary part of the self-energy diagrams. We begin with the tree-level rate, corresponding, in the unitary gauge, to the single two-loop diagram in Fig. 1.

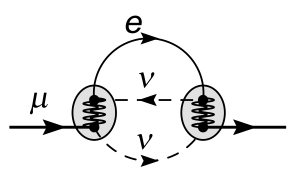

Fig. 1. Diagram corresponding to the tree-level decay $\mu \to e, \nu, \nu$.

It is convenient to use a Fierz transformed diagram (Fig. 2). For the full decay width and with $M_W \to \infty$ we have

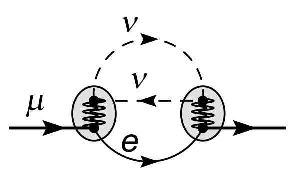

Fig. 2. Fierz-transformed diagram.

$$\Gamma^{(0)} = \frac{\mathrm{Im}\Sigma}{M}\,,$$

$$\begin{aligned} i\Sigma \;=\; & -\frac{1}{2}\mathrm{Tr}\int \frac{d^D k_1 d^D k_2}{(2\pi)^{2D}}\,(\not{p}+M)\left(\frac{ig_w}{2\sqrt{2}}\gamma^\alpha(1-\gamma_5)\right) \\ & \times\left(\frac{-i(\not{k}_1+m)}{k_1^2-m^2+i\delta}\right)\left(\frac{ig_w}{2\sqrt{2}}\gamma^\beta(1-\gamma_5)\right)\left(\frac{-i\not{k}_2}{k_2^2+i\delta}\right)\left(\frac{ig_w}{2\sqrt{2}}\gamma^\nu(1-\gamma_5)\right) \\ & \times\left(\frac{-i(\not{p}-\not{k}_1+\not{k}_2)}{(p-k_1+k_2)^2+i\delta}\right)\left(\frac{ig_w}{2\sqrt{2}}\gamma^\mu(1-\gamma_5)\right)\left(\frac{ig_{\alpha\mu}}{M_W}\right)\left(\frac{ig_{\beta\nu}}{M_W}\right). \end{aligned} \quad (2)$$

After evaluating the trace and the Wick rotation we obtain a result in terms of an integral with the following propagator factors (Fig. 3): $[1] = k_1^2 + m^2$, $[2] = k_2^2$, $[5] = (p - k_1 + k_2)^2$. We identify two contributing regions of the loop momenta:

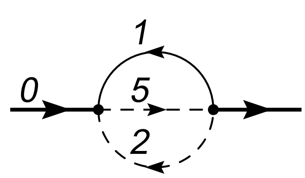

Fig. 3. Initial integral (solid thin line — mass m, solid thick line — mass M).

Region 1 (Fig. 4)	$\lvert k_1\rvert \gg m$	$[1] \to k_1^2$
Region 2 (Fig. 5)	$\lvert k_1\rvert \sim m$	$[5] \to (p+k_2)^2$

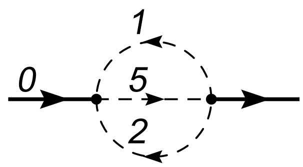

Fig. 4. Region 1 ($|k_1| \gg m$).

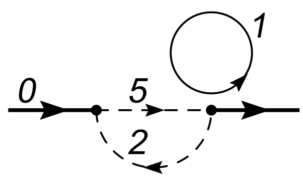

Fig. 5. Region 2 ($|k_1| \sim m$).

In the first region (Fig. 4) we have a two-loop massless integral,

$$\frac{\mathrm{Im}\Sigma^{(1)}}{\mathcal{F}_0^2 M^{1-2\epsilon}\Gamma_0} \;=\; -\frac{12}{\epsilon}\rho^4 + 1 - 8\rho^2 - 24\rho^4 + 16\rho^6. \tag{3}$$

The fractional power of M arises because the external momentum $p^2 = -M^2$ is the only scale of the D-dimensional integrals. In the second region (Fig. 5) after averaging over the directions of k_1 the integral factorizes into a one-loop vacuum bubble and a one-loop propagator-type integral,

$$\frac{\mathrm{Im}\Sigma^{(2)}}{\mathcal{F}_0^2 M m^{-2\epsilon}\Gamma_0} \;=\; \frac{12}{\epsilon}\rho^4 + 24\rho^4 - 8\rho^6. \tag{4}$$

Note that the fractional power now is that of m. After adding the contributions and expanding the ϵ-powers of masses, we obtain a series expansion of the decay width in powers and logarithms of the electron-to-muon mass ratio,

$$\begin{aligned}\Gamma^{(0)}(\mu \to e,\nu,\nu) \;&=\; \frac{\mathrm{Im}(\Sigma^{(1)} + \Sigma^{(2)})}{M} \\ &\stackrel{\epsilon\to 0}{\longrightarrow} \Gamma_0\left\{1 - 8\rho^2 - 24\rho^4\log\rho + 8\rho^6\right\}.\end{aligned} \tag{5}$$

The finite logarithmic term is a remnant of divergences in both regions.

4. $\mathcal{O}(\alpha)$ correction to the muon decay

The $\mathcal{O}(\alpha)$ correction is more challenging since it receives contributions from three three-loop diagrams, as well as two renormalization terms (Fig. 6). As before we use the Fierz transformed "charge retention" diagrams.

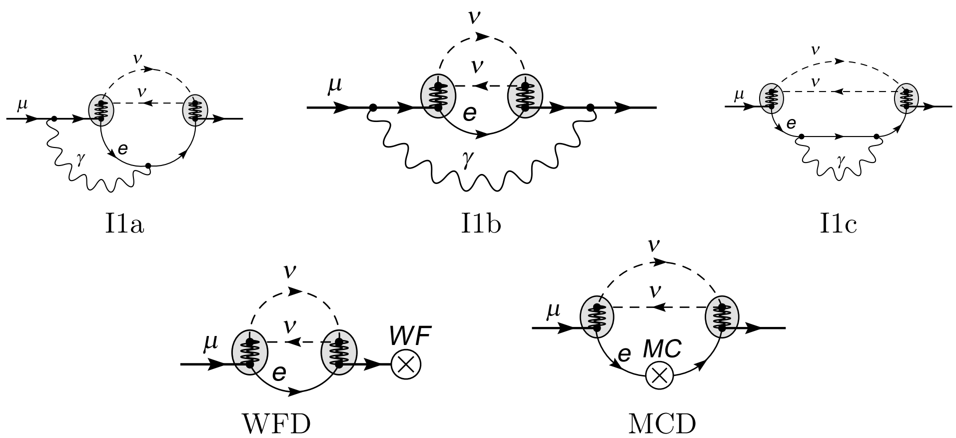

Fig. 6. $\mathcal{O}(\alpha)$ diagrams.

4.1. Renormalization terms

The one-loop wave-function renormalization constant and the mass counterterm are given by

$$\mathrm{WF} \;=\; -\mathcal{F}_0 M^{-2\epsilon}\frac{\alpha}{4\pi}\left\{\frac{3}{\epsilon}+4+8\epsilon+\mathcal{O}(\epsilon^2)\right\}, \tag{6}$$

$$\mathrm{MC} \;=\; i\mathcal{F}_0 m^{1-2\epsilon}\frac{\alpha}{4\pi}\left\{\frac{3}{\epsilon}+4+8\epsilon+\mathcal{O}(\epsilon^2)\right\}. \tag{7}$$

Their contributions are found using the same technique as in Section 3. In the present case we need to keep an extra power of ϵ since the renormalization constants are divergent. We find

$$\begin{aligned}\frac{\mathrm{Im}(\mathrm{WFD}^{(1)}+\mathrm{WFD}^{(2)})}{M\Gamma_0\alpha/\pi} \quad &\overset{\epsilon\longrightarrow 0}{\longrightarrow} \frac{1}{\epsilon}\left(-\frac{3}{4}+6\rho^2+18\rho^4\log\rho-6\rho^6\right)\\ &-\frac{85}{16}+3\log M+38\rho^2+24\rho^2\log\rho\\ &+\rho^4\left(\frac{45}{2}+60\log\rho-18\log^2\rho+72\log^2 M-6\pi^2\right)\\ &+\rho^6\left(6-12\log\rho+24\log M\right),\end{aligned} \tag{8}$$

$$\frac{\mathrm{Im}(\mathrm{MCD}^{(1)} + \mathrm{MCD}^{(2)})}{M\Gamma_0\alpha/\pi} \overset{\epsilon\to 0}{\longrightarrow} \frac{1}{\epsilon}\left(12\rho^2 + 18\rho^4 + 72\rho^4 \log\rho - 36\rho^6\right)$$
$$+\rho^2\left(76 - 24\log\rho - 48\log M\right)$$
$$+\rho^4\left(150 + 168\log\rho - 216\log^2\rho - 72\log M\right.$$
$$\left.+864\log^2 M - 24\pi^2\right)$$
$$+\rho^6\left(24 + 144\log M\right). \tag{9}$$

It now remains to find the genuine $\mathcal{O}(\alpha)$ corrections described by three-loop diagrams.

4.2. Asymptotic expansion regions

The three-loop diagrams I1a, I1b, and I1c in Fig. 6 are special cases of one basic topology (see Fig. 7), with $[1] = (p + k_3 - k_2)^2$, $[3] = k_2^2 + m^2$, $[4] = k_1^2 + m^2$, $[6] = k_3^2$, $[7] = (k_1 - k_2)^2$, and $[8] = (p + k_1 - k_2)^2 + M^2$. Since this topology involves two different mass scales, we again analyze how

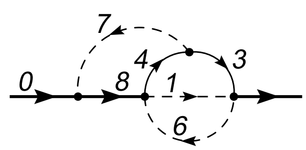

Fig. 7. Initial topology (solid thin line — mass m, solid thick line — mass M).

to factorize it into single-scale contributions. Four regions of virtualities contribute to the imaginary part of such diagrams:

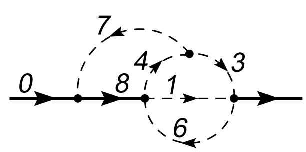

Fig. 8. Region 1 ($|k_1| \gg m$, $|k_2| \gg m$).

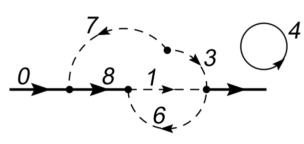

Fig. 9. Region 2 ($|k_1| \sim m$, $|k_2| \gg m$).

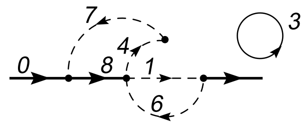

Fig. 10. Region 3 ($|k_1| \gg m$, $|k_2| \sim m$).

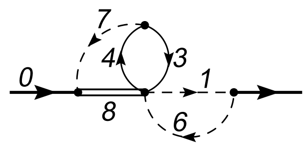

Fig. 11. Region 4 ($|k_1| \sim m$, $|k_2| \sim m$).

Region 1 (Fig. 8)	$|k_1| \gg m$, $|k_2| \gg m$	$[3] \to k_2^2$ $[4] \to k_1^2$
Region 2 (Fig. 9)	$|k_1| \sim m$, $|k_2| \gg m$	$[3] \to k_2^2$ $[7] \to k_2^2$ $[8] \to (p-k_2)^2 + M^2$
Region 3 (Fig. 10)	$|k_1| \gg m$, $|k_2| \sim m$	$[4] \to k_1^2$ $[1] \to (p+k_3)^2$ $[7] \to k_1^2$ $[8] \to (p+k_1)^2 + M^2$
Region 4 (Fig. 11)	$|k_1| \sim m$, $|k_2| \sim m$	$[1] \to (p+k_3)^2$ $[8] \to 2p(k_1-k_2) + i\delta$

Each diagram will include contributions from all regions, *e.g.* $\mathrm{I1a} = \mathrm{I1a}^{(1)} + \mathrm{I1a}^{(2)} + \mathrm{I1a}^{(3)} + \mathrm{I1a}^{(4)}$. In the following, the calculations in all four regions are sketched.

Region 1

The one-loop subgraph with massless propagators [1] and [6] can be integrated. After that, we have a two-loop topology which has been solved in [7]. The results for the three diagrams are

$$\begin{aligned}\frac{\mathrm{Im}(\mathrm{I1a}^{(1)})}{X} &= -\frac{15}{\epsilon^2}\rho^4 + \frac{1}{\epsilon}\left(\frac{1}{2} - 4\rho^2 + 3\rho^4 + 33\rho^6\right) \\ &\quad + \frac{121}{24} - \frac{\pi^2}{2} - \frac{76}{3}\rho^2 + \rho^4\left(9\pi^2 - \frac{465}{2}\right) - \frac{451}{6}\rho^6, \quad (10)\end{aligned}$$

$$\frac{\mathrm{Im}(\mathrm{I1b}^{(1)})}{X} = -\frac{6}{\epsilon^2}\rho^4 + \frac{1}{\epsilon}\left(\frac{1}{2} - 4\rho^2 - \frac{75}{2}\rho^4 + 6\rho^6\right) + \frac{275}{2} - \frac{121}{3}\rho^2 + \rho^4\left(12\pi^2 - \frac{387}{2}\right) + 7\rho^6, \tag{11}$$

$$\frac{\mathrm{Im}(\mathrm{I1c}^{(1)})}{X} = -\frac{6}{\epsilon^2}\rho^4 + \frac{1}{\epsilon}\left(-\frac{1}{4} - 10\rho^2 - \frac{75}{2}\rho^4 + 12\rho^6\right) - \frac{7}{3} - \frac{247}{3}\rho^2 + \rho^4\left(12\pi^2 - \frac{333}{2}\right) + 33\rho^6, \tag{12}$$

$$X = \frac{\mathcal{F}_0^3 M^{1-4\epsilon}\mathit{\Gamma}_0\alpha}{\pi}. \tag{13}$$

The Region 1 is technically the hardest. In all remaining ones there is some degree of factorization which simplifies the calculations.

Region 2

After averaging over the directions of momentum k_1 we can integrate the one-loop massive bubble [4]. The remainder is a two-loop diagram, in which again we can first integrate the massless propagators [1] and [6]. The last integration is one-loop, and we find

$$\frac{\mathrm{Im}(\mathrm{I1a}^{(2)})}{Y} = \frac{18}{\epsilon^2}\rho^4 + \frac{1}{\epsilon}\left(27\rho^4 - \frac{67}{3}\rho^6\right) + \rho^4(162 - 18\pi^2) - \frac{113}{18}\rho^6, \tag{14}$$

$$\frac{\mathrm{Im}(\mathrm{I1b}^{(2)})}{Y} = \frac{6}{\epsilon^2}\rho^4 + \frac{1}{\epsilon}\left(\frac{75}{2}\rho^4 - 2\rho^6\right) + \rho^4(\frac{657}{4} - 6\pi^2) - \frac{20}{3}\rho^6, \tag{15}$$

$$\frac{\mathrm{Im}(\mathrm{I1c}^{(2)})}{Y} = -\frac{21}{\epsilon^2}\rho^4 + \frac{1}{\epsilon}\left(-\frac{105}{2}\rho^4 + 52\rho^6\right) + \rho^4(21\pi^2 - \frac{657}{4}) + \frac{40}{3}\rho^6, \tag{16}$$

$$Y = \frac{\mathcal{F}_0^3 m^{-2\epsilon} M^{1-2\epsilon}\mathit{\Gamma}_0\alpha}{\pi}. \tag{17}$$

Region 3

In this region we average over k_2 directions, integrate the massive bubble with [3], and the rest factorizes into two one-loop integrals. This region gives a non-zero contribution only for I1a,

$$\frac{\mathrm{Im}(\mathrm{I1a}^{(3)})}{Y} = \frac{6}{\epsilon^2}\rho^4 - \frac{43}{3\epsilon}\rho^6 + \rho^4\left(18 - 2\pi^2\right) - \frac{301}{18}\rho^6. \tag{18}$$

Region 4

Finally, in this last region, after we integrate [1] and [6], we are left with an "eikonal" integral [8]. Again, a solution was found in [7]. We obtain

$$\begin{aligned}\frac{\mathrm{Im}(\mathrm{I1a}^{(4)})}{Z} &= -\frac{1}{\epsilon^2}\left(9\rho^4+16\rho^6\right)-\frac{1}{\epsilon}\left(30\rho^4+29\rho^6\right)\\ &\quad +16\pi^2\rho^3+\left(3\pi^2-84\right)\rho^4+16\pi^2\rho^5+\left(\frac{16}{3}\pi^2-\frac{1175}{18}\right)\rho^6,\end{aligned} \tag{19}$$

$$\frac{\mathrm{Im}(\mathrm{I1b}^{(4)})}{Z} = 0\,, \tag{20}$$

$$\frac{\mathrm{Im}(\mathrm{I1c}^{(4)})}{Z} = \frac{27}{\epsilon^2}\rho^4+\frac{1}{\epsilon}\left(72\rho^4-30\rho^6\right)+\left(192-9\pi^2\right)\rho^4-68\rho^6\,, \tag{21}$$

$$Z = \frac{\mathcal{F}_0^3 m^{-4\epsilon} M\Gamma_0\alpha}{\pi}\,. \tag{22}$$

4.3. Total result for the $\mathcal{O}(\alpha)$ corrections

In the sum of the contributions of all four regions we can take the limit $\epsilon\to 0$. The result is finite,

$$\begin{aligned}\Gamma^{(1)}(\mu\to e,\nu,\nu) &= \frac{\mathrm{Im}(\mathrm{WFD}+\mathrm{MCD}+\mathrm{I1a}+\mathrm{I1b}+\mathrm{I1c})}{M}\\ &\xrightarrow{\epsilon\to 0} \Gamma_0\left(\frac{\alpha}{\pi}\right)\left\{\left(\frac{25}{8}-\frac{\pi^2}{2}\right)-\rho^2\left(34+24\log\rho\right)\right.\\ &\quad +16\pi^2\rho^3-\rho^4\left(8\pi^2+\frac{273}{2}-36\log\rho+72\log^2\rho\right)\\ &\quad \left.+16\pi^2\rho^5-\rho^6\left(\frac{526}{9}-\frac{152}{3}\log\rho\right)+\mathcal{O}\left(\rho^8\right)\right\}.\end{aligned} \tag{23}$$

and we now see that quadratic logarithmic terms are present, reflecting $1/\epsilon^2$ divergences in the partial results. The result coincides with the expansion of the known formula [9] in which the mass dependence was included exactly.

For the muon decay the expansion parameter ρ is small and allows us to neglect all terms except for the first one which corresponds to the massless electron limit. In case of the quark decays the situation may change significantly since the expansion parameter is larger, $\rho\simeq 0.27$ and even in the example above the mass effects increase the decay rate by about 10 percent. Additional enhancement of the mass effects is expected in the decay $b\to c\bar{c}S$, where two massive particles are present in the final state.

5. Summary

In this talk, we have demonstrated how the mass dependence of the decay width can be obtained using the asymptotic operation. The advantage of the method is that at every stage of loop calculations we deal with relatively simple one-scale integrals, which, using recurrence relations, can be reduced to master integrals. Those can be determined analytically, at least in the present problem.

In the future application of this method to the non-leptonic decays involving two heavy quarks in the final state, we anticipate convergence problems if the Coulomb singularity is an important effect. If this turns out to be the case, a threshold expansion can be employed [10, 11]. In fact, it may be feasible to use both expansion schemes and match the two results for moderate values of the charm mass.

We anticipate that the evaluation of the charm mass effects, together with a determination of the scale of the strong coupling constant, will yield a precise theoretical prediction for the semileptonic branching ratio of the b quark. If similar progress is made in experimental studies, it will then be possible to confront them with the Standard Model and discover or constrain "new physics" effects. Since the Standard Model decays of b are strongly suppressed by the smallness of V_{cb}, the semileptonic branching ratio may become a uniquely sensitive probe of exotic phenomena.

This research was supported by the Science and Engineering Research Canada. We thank Ian Blokland for many helpful discussions.

REFERENCES

[1] I.I.Y. Bigi, B. Blok, M.A. Shifman, A.I. Vainshtein, *Phys. Lett.* **B323**, 408 (1994).

[2] A.H. Mahmood *et al.*, *Phys. Rev.* **D70**, 032003 (2004).

[3] A. Czarnecki, M. Ślusarczyk, F.V. Tkachov, `hep-ph/0511004`.

[4] M.B. Voloshin, *Phys. Rev.* **D51**, 3948 (1995).

[5] M.B. Voloshin, *Int. J. Mod. Phys.* **A11**, 4931 (1996).

[6] F.V. Tkachev, *Sov. J. Part. Nucl.* **25**, 649 (1994).

[7] I.R. Blokland, Ph.D. thesis, University of Alberta, 2004, UMI-NQ-95909.

[8] A. Czarnecki, V. Smirnov, *Phys. Lett.* **B394**, 211 (1997).

[9] Y. Nir, *Phys. Lett.* **B221**, 184 (1989).

[10] M. Beneke, V.A. Smirnov, *Nucl. Phys.* **B522**, 321 (1998).

[11] A. Czarnecki, K. Melnikov, *Phys. Rev. Lett.* **80**, 2531 (1998).